JCTC Journal of Chemical Theory and Computation

pubs.acs.org/JCTC Article

Water in an External Electric Field: Comparing Charge Distribution Methods Using ReaxFF Simulations

Jason P. Koski,* Stan G. Moore, Raymond C. Clay, Kurt A. O'Hearn, H. Metin Aktulga, Mark A. Wilson, Joshua A. Rackers, J. Matthew D. Lane, and Normand A. Modine

Cite This: J. Chem. Theory Comput. 2022, 18, 580−594 Read Online

ACCESS | Metrics & More | Article Recommendations | Supporting Information

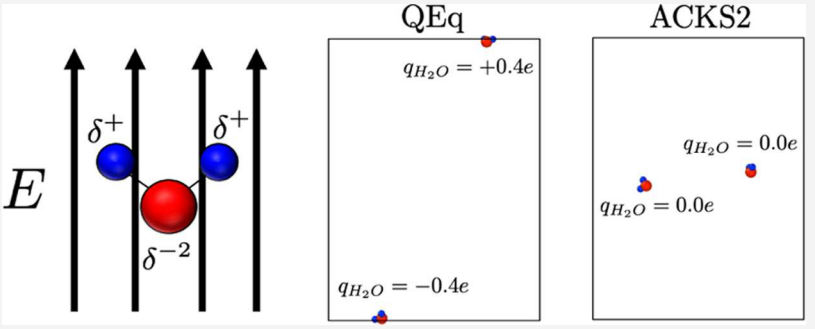

ABSTRACT: The growing interest in the effects of external electric fields on reactive processes requires predictive methods that can reach longer length and time scales than quantum mechanical simulations. Recently, many studies have included electric fields in ReaxFF, a widely used reactive molecular dynamics method. In the case of modeling an external electric field, the charge distribution method used in ReaxFF is critical. The most common charge distribution method used in previous studies of electric fields is the charge equilibration (QEq) method, which assumes that the system is a contiguous conductor and that charge transfer can occur across any distance. In contrast, many systems of interest are insulators or semiconductors, and long-distance charge transfer should not occur in response to a small difference in potential. This study focuses on the limitations of the QEq method in the context of water in an external electric field. We demonstrate that QEq can predict unphysical charge distributions and exhibits properties that do not converge as a function of system size. Furthermore, we show that electric fields within the recently developed atom-condensed Kohn-Sham density functional theory (DFT) approximated to the second-order (ACKS2) approach address the major limitations of electric fields in QEq. With ACKS2, we observe more physical charge distributions and properties that converge as a function of system size. We do not suggest that ACKS2 is perfect in all circumstances but rather show specific cases where it addresses the major shortcomings of QEq in the context of an external electric field.

I. INTRODUCTION

In recent years, there is a growing interest in the role of external electric fields on reactive processes because external electric fields offer a mechanism to alter reaction rates, control selectivity, and promote molecular dissociation.[1−5] For example, the presence of an external electric field can promote the dissociation of water and thus influence a system's pH, which has critical implications in realms such as neuroscience and electrochemistry[6] but is relevant to any field or application where water is an active solvent. Reactive molecular dynamics (MD) is appealing for modeling these systems because it allows for simulations with bond breaking and reactivity with length and times scales that are orders of magnitude larger than what is tractable in quantum mechanical (QM) simulations. ReaxFF is a popular reactive molecular dynamics formalism that calculates a bond order that depends on the interatomic distance and has been applied to a plethora of research fields[7,8] including catalysis, atomic layer deposition, high-energy materials, and interfacial chemistry, such as molecular adsorption and desorption from high-current-carrying conductor/oxide surfaces.[9,10] An important aspect of ReaxFF is its support for dynamically updating per-atom partial charges. The rearrangement and redistribution of charge in each system provide the capability to model reactive processes. In this paper, we focus on the importance of the charge distribution method in ReaxFF for describing systems under an externally applied electric field.

The most common charge distribution method used with ReaxFF is the charge equilibration (QEq) method,[11] where the

Received: September 27, 2021
Published: December 16, 2021

https://doi.org/10.1021/acs.jctc.1c00975
J. Chem. Theory Comput. 2022, 18, 580−594

electrostatic energy is minimized with respect to atomic charge at each molecular dynamics (MD) step, with the constraint that the system is electroneutral (see the Section II for additional details). The related electronegativity equalization method (EEM)[12] formulates the charge distribution problem slightly differently from QEq but, in practice, delivers the same results. The main difference is that QEq replaces the point-charge interactions in EEM by interactions between Slater-like electron densities. The other difference is that QEq can include a cubic term for hydrogen, but it is rarely used in practice. QEq has notable shortcomings, including predictions of noninteger charges of dissociated species[13,14] and inaccurate descriptions for molecular polarization.[7,14] These artifacts stem from the assumption that the system is a perfect conductor where there is no charge-transfer penalty as a function of distance. This shortcoming of the QEq method leads to unphysical charge transfer between molecules separated by large distances.

The first study to use electric fields in ReaxFF simulations was conducted by Assowe et al.,[15] where they observed enhanced corrosion of a Ni(111) surface by water as a function of electric field strength. In this study, they use the QEq method and introduce the effect of the electric field on the charge distribution by including the electric field potential in the total electrostatic energy proposed by Chen and Martínez.[16] A mathematical description of this is provided in the Section II. Since then, the vast majority of ReaxFF studies with an external electric field use QEq,[17−31] though to the best of our knowledge, a thorough investigation of the limitations of this approach does not exist.

Aside from the QEq studies, a few recent studies apply the charge transfer with polarization current equalization (QTPIE) method[13] to study the effect of an external electric field within the ReaxFF framework.[32−34] The QTPIE method is an extension of the QEq method that introduces a charge-transfer cutoff that, in principle, addresses the primary global charge-transfer shortcoming of QEq. The primary drawback of the QTPIE method is that it is formulated based on physical intuition rather than rigorously derived; a distance-dependent function is introduced by which long-range charge transfer is penalized. QTPIE also uses an effective atomic electronegativity that depends on the relative distance between atom-neighbor pairs.[35,36]

The atom-condensed Kohn-Sham density functional theory (DFT) approximated to second-order (ACKS2) approach[14] can be shown as a generalization of EEM that, similar to QTPIE, impedes long-range charge transfer. However, unlike QTPIE, ACKS2 is rigorously derived from DFT. This improved accuracy comes with a cost: QEq and QTPIE require solving an $N \times N$ symmetric, positive definite linear system of equations, normally iteratively, using a solver such as the standard conjugate-gradient (CG), while ACKS2 requires solving a larger $2N + 2 \times 2N + 2$ symmetric, indefinite system and also using a more complex solver such as biconjugate gradient-stabilized (BiCGStab).[37] Here, N is the number of atoms in the system. Unfortunately, the use of ACKS2 has been limited due to the low transferability of QEq force fields to ACKS2. ACKS2 has been implemented in the Amsterdam density functional (ADF) code and in the Purdue reactive molecular dynamics (PuReMD) software.[38] As part of this work, ACKS2 was also implemented in LAMMPS[39,40] (now available in the public source code), compatible with MPI, as well as graphics processing units (GPUs) through the Kokkos performance portability library.[41−43] ACKS2 in LAMMPS has been benchmarked on central processing unit (CPU) and GPU hardware.[44] This fully parallelized version in LAMMPS was based on a serial version of ACKS2 in the PuReMD code.[37] There have been no published studies to the best of our knowledge that use ACKS2 with an externally applied electric field.

In this paper, we evaluate and compare the QEq and ACKS2 charge distribution methods in the context of water in an external electric field. We introduce the electric field into the ReaxFF framework, as was proposed by Chen and Martínez[16] and first implemented by Assowe et al.[15] Section II describes the details of the methods used in this study, namely, ReaxFF, DFT, and an unrestricted Hartree−Fock (UHF) quantum chemistry formalism. In this section, we provide additional details of the QEq and ACKS2 charge distribution methods. In Section III, we apply an electric field to water in several test problems: two water molecules, one molecular water, one dissociated water, constant volume simulations of a bulk water slab, and constant pressure simulations of bulk water confined between two hard walls in the direction of the applied electric field. Finally, in Section IV, we present our conclusions based on the results shown in Section III. In general, we find that the global charge transfer in QEq is exacerbated with an electric field as we observe unphysical charge distributions. The QEq charge distributions interact with the electric field to produce unphysical forces and stresses and, hence, unrealistic dynamics. We also observe nonconverging behavior as a function of system size for bulk water in an electric field when using QEq. This is particularly troubling because molecular simulations often assume convergence to bulk system properties with increasing system size. On the other hand, ACKS2 charge distributions are affirmed with comparisons to both quantum chemistry and DFT calculations.

II. METHODS

II.I. ReaxFF. The ReaxFF force field was developed by van Duin et al.,[45] where the bond order between a pair of atoms is dependent on the interatomic distance. The bond order calculation allows for reactivity and bond breaking to take place during the MD simulation. The ReaxFF force field is composed of several energy terms

$$E_{\text{system}} = E_{\text{bond}} + E_{\text{vdW}} + E_{\text{Coulomb}} + E_{\text{pol}} + E_{\text{val}} + E_{\text{tors}} + E_{\text{under}} + E_{\text{over}} + E_{\text{lp}} + E_{\text{H-bond}} + E_{\text{pen}} + E_{\text{3conj}} + E_{\text{4conj}} \quad (1)$$

where E_{bond} is the bond energy, E_{vdW} is the van der Waals energy, E_{Coulomb} is the Coulomb energy, E_{pol} is the self-polarization energy in distributing charges to atoms, E_{val} is the valence angle energy, E_{tors} is the torsion angle energy, E_{under} is the undercoordination penalty energy, E_{over} is the overcoordination penalty energy, E_{lp} is the lone-pair energy, $E_{\text{H-bond}}$ is the hydrogen bond energy, E_{pen} is the penalty energy from stabilizing double bonds in three-body interactions, and E_{3conj} and E_{4conj} are the energies from conjugation in three- and four-body interactions, respectively.

In all ReaxFF simulations, we use the LAMMPS software package equipped with the REAXFF package[46] (previously named the USER-REAXC package). In addition to the "fix qeq/reaxff" command to run ReaxFF with QEq, we have further developed the code to now include a "fix acks2/reaxff" command to run ReaxFF with ACKS2. The incorporation of the electric field within ReaxFF simulations via eq 4 is now released publicly in the LAMMPS source code. In all ReaxFF

https://doi.org/10.1021/acs.jctc.1c00975
J. Chem. Theory Comput. 2022, 18, 580−594

simulations, we use a time step of 0.2 fs and a charge distribution tolerance of 1×10^{-10}. The Coulomb cutoff is set to 10 Å.

The ReaxFF force fields used for this study are provided in the Supporting Information and based on the force field used in Achtyl et al.[47] In general, the QEq water force field is trained for density and diffusion. For the ACKS2 force field, two ACKS2-specific parameters were tuned against the same training data via a relatively simple single-parameter-at-a-time search while keeping the same QEq water force field parameters for the rest. A more rigorous ACKS2 force field would require a full reparameterization against the training data that includes the atomic parameters, bonded parameters, angle parameters, etc. As such, the fitting of the ACKS2 parameters will cause deviations from the QEq water behavior, where the full QEq parameterization was optimized against the DFT training data.

II.II. QEq. At every MD time step, the atomic charge distribution must be updated for ReaxFF to achieve sufficient simulation accuracy. As such, ReaxFF is oftentimes coupled with a global charge model. One of the earliest models used with ReaxFF was QEq. In QEq, the charges $\mathbf{q} = \{q_1, ..., q_N\}$, where N is the number of atoms, are updated by minimizing the electrostatic energy with the constraint that the system remains charge neutral

$$\min_{\mathbf{q}} \quad E_{\text{ele}}(\mathbf{q}) = \sum_{i}^{N} \chi_i q_i + \frac{1}{2} \sum_{i,j}^{N} H_{ij} q_i q_j$$
$$\text{subject to} \quad \sum_{i}^{N} q_i = 0 \tag{2}$$

where

$$H_{ij} = \delta_{ij}\eta_i + (1 - \delta_{ij}) \cdot F_{i,j}$$
$$F_{i,j} = \begin{cases} \dfrac{T(r_{ij}) \cdot k_c}{\sqrt[3]{r_{ij}^3 + \gamma_{ij}^{-3}}}, & r_{ij} \le r_{\text{nonb}} \\ 0, & \text{otherwise} \end{cases}$$

In the above, q_i is the charge of each atom i, r_{ij} is the distance between atom i and atom j, r_{nonb} is the long-ranged cutoff (typically valued at 10−12 Å), δ_{ij} denotes the Kronecker δ operator, χ_i is the Mulliken electronegativity of atom i, η_i is twice the atomic Parr−Pearson hardness, k_c is the Coulomb constant in a vacuum, $T(r_{ij})$ is a seventh-order taper function, and γ_{ij} is the shielding parameter between atoms i and j. Numerically, this minimization problem can be recast as the problem of finding the solution to two decoupled sparse systems of linear equations using the method of Lagrange multipliers. The work in developing optimized solvers for global charge models together with ReaxFF has been studied elsewhere.[37,48,49]

The two main approximations in QEq are apparent in eq 2: (1) the term $\eta_i q_i^2$ (note that $H_{ii}q_i^2 = \eta q_i^2$) is consistent with a uniform density of states near the Fermi level, and thus the charge-transfer properties of the system are characteristic of a metal. An insulator such as water, or any other system with gaps in its density of states, should have derivative discontinuities in the expression for its energy as a function of charge. (2) The term $T(r_{ij})$ smoothly truncates the Coulomb interactions in the system. This approximation is inherent within the common implementation of the ReaxFF formalism (i.e., eq 2), though we discuss its implications here in the context of QEq. The truncation of the Coulomb interactions has a profound effect when dealing with sheets of charge, such as when an electric field is applied to a dielectric, since it replaces a constant field that extends to infinite distances with a short-ranged field. In some cases, such as the potential within a dielectric slab in an applied field, the effects of these approximations cancel out, resulting in surprisingly reasonable behavior. In other cases, such as the charge distribution or forces in the same dielectric slab, the effects of these approximations reinforce each other to produce completely unphysical behavior. We will explore these cases in Section III.IV.

II.III. ACKS2. The ACKS2 method[14] was introduced as an extension of EEM, which is closely related to QEq. ACKS2 was developed with the aim of more correctly modeling dipoles and charge transfer during bond formation/dissociation via additional empirically fitted parameters. We note that other methods such as the atom−atom charge-transfer (AACT) method,[50,51] split charge equilibration (SQE),[51−54] and the previously mentioned QTPIE method are all alternatives to EEM, with the aim of addressing the limitations of EEM (and QEq). However, unlike ACKS2, these methods are not rigorously derived from DFT and an exploration of these methods in the context of an external electric field is beyond the scope of this work. In addition to the original ACKS2 paper, we point the reader to a subsequent ACKS2 paper[55] (also by Verstraelen) that was published to more clearly motivate the ACKS2 model and to simplify the derivation as much as possible. In this subsequent ACKS2 paper, the direct approximation of the KS-DFT response theory is more readily understood.

Minimizing electrostatic energy with the additional constraints introduced by the second-order approximation of the Kohn−Sham potential, the following linear system is obtained

$$\begin{bmatrix} \mathbf{H} & \mathbf{I}_n & \mathbf{1}_n & \mathbf{0}_n \\ \mathbf{I}_n & \mathbf{X} & \mathbf{0}_n & \mathbf{1}_n \\ \mathbf{1}_n^{\mathrm{T}} & \mathbf{0}_n^{\mathrm{T}} & 0 & 0 \\ \mathbf{0}_n^{\mathrm{T}} & \mathbf{1}_n^{\mathrm{T}} & 0 & 0 \end{bmatrix} \begin{bmatrix} \mathbf{q} \\ \mathbf{U} \\ \mu_{\text{mol}} \\ \lambda_U \end{bmatrix} = \begin{bmatrix} -\boldsymbol{\chi} \\ \mathbf{0} \\ q_{\text{net}} \\ 0 \end{bmatrix} \tag{3}$$

where

$$X_{ij} = \begin{cases} \left\{ \begin{cases} \Lambda \cdot \left(\dfrac{r_{ij}}{\sigma_{ij}}\right)^3 \cdot \left(1 - \dfrac{r_{ij}}{\sigma_{ij}}\right)^6, & r_{ij} \le r_{\text{min}},\ X_{ij} > 0 \\ 0, & \text{otherwise} \end{cases} \right\} & i \ne j \\ \displaystyle\sum_{j=1}^{i-1} - X^{ij}, & i = j \end{cases}$$

In the above, $\mathbf{U}$ contains Kohn-Sham potential coefficients, μ_{mol} and λ_{U} are Lagrangian multipliers from the underpinning optimization problem, X contains terms for the linear response kernel of the Kohn-Sham potential, q_{net} is the net charge on the atomic system, and $\mathbf{H}$ and $\boldsymbol{\chi}$ contain the coefficients as defined by the QEq method. Also, $\sigma_{ij} = \frac{\sigma_i + \sigma_j}{2}$ and $r_{\text{min}} = \min\{r_{\text{nonb}}, \sigma_{ij}\}$, where the parameters σ_i and Λ are ACKS2-specific such that the σ_i parameters are based on element types, and Λ is a global bond softness parameter. Lastly, note that incorporating the ACKS2 method adds additional contributions to the Coulomb and polarization terms in the ReaxFF formulation.[14]

In addition to using a second-order approximation of the Kohn-Sham potential, another approximation in ACKS2 is the

https://doi.org/10.1021/acs.jctc.1c00975
J. Chem. Theory Comput. 2022, 18, 580−594

use of a simple exponential decay to zero at large interatomic separations between two fragments for the Kohn-Sham linear response matrix; the exact relation is not trivial. Furthermore, the truncation of the Coulomb interactions generally used in the ReaxFF framework creates its own inaccuracies in the context of ACKS2. Specifically, the short-ranged charge transfer coupled with the short-ranged Coulomb interactions results in an inability to accurately model both the charge distribution and the screening of an electric field if the system is larger than the Coulomb cutoff. We will demonstrate this phenomenon in Section III.IV.

II.IV. External Electric Fields with Charge Models. We introduce the electric field by including the electric field potential in the electrostatic energy. This is given by

$$E_{ele}(\mathbf{q}, E_{el}) = E^0_{ele}(\mathbf{q}) - \sum_{i=1}^{N} q_i R_i \cdot E_{el} \tag{4}$$

In the above, $\vec{R}_i$ is the absolute position of each atom i, and $\vec{E}_{el}$ is the electric field vector. The inclusion of the electric field potential in the electrostatic energy introduces both a force from the electric fields on each atom, $\vec{F}_{i,el} = q_i\vec{E}_{el}$, and an additional contribution to the charge distribution. Without the inclusion of the electric field potential in eq 4, the charge distribution would neglect the external electric field and only be a function of the electronegativity, atomic hardness, and Coulomb terms. The introduction of an external electric field affects the distribution of atomic charge and creates an internal field that opposes the external field.

As mentioned previously, we introduce the external electric field following the formalism proposed by Chen and Martínez[16] and first implemented in the context of ReaxFF by Assowe et al.[15] In these papers, they introduce the electric field via a modification to the electronegativity $\chi_i = \chi_i - \sum_{i=1}^{N}\vec{R}_i \cdot \vec{E}_{el}$, which we note is mathematically equivalent to eq 4 above. For the remainder of the paper, we assume that the electric field is applied in the z-direction and indicates its magnitude by E. For brevity, we will also indicate the z-component of the position of atom i or molecule i as z_i.

The application of the electric field via eq 4 leads to a dependence on the absolute position, and it is nontrivial how to treat certain aspects of the simulation when an atom crosses a boundary that corresponds to the electric field direction. For example, if we use the absolute "unwrapped" position of the atom when it crosses a periodic boundary, atoms that are further up the field would interact with atoms that are further down the field, leading to a large Coulombic interaction. If we use the local "wrapped" position of the atom, we could see discontinuities in things like the system's dipole moment or run into issues such as atoms in the same molecules that see dramatically different potentials when the molecule has only partially crossed the boundary. Here, we avoid these potential issues by using periodic boundary conditions in the x- and y-directions and a fixed boundary condition with a reflective wall in the z-direction. The reflective wall in the z-direction ensures no atom can cross the boundary in the direction of the applied field. Furthermore, we set the z-image flags to 0. Interestingly, there is a possible way to address this issue through an effective atomic electronegativity that uses the relative distance between atom-neighbor pairs,[35,36] as was done by Kritikos and Giusti,[34] but a full exploration of this method was beyond the scope of this work.

II.V. DFT. For comparison to our ReaxFF calculations, we ran Kohn-Sham density functional theory (DFT)[56] calculations using version 5.4.4 of the Vienna ab initio simulation package (VASP).[57−60] Although various forms of van der Waals dispersion corrections are available in VASP, we were interested in the qualitative charge transfer and polarization properties of water in an electric field rather than the detailed structure of water, where van der Waals dispersion would be expected to have a significant role. Therefore, our calculations used the well-established Perdew−Burke−Ernzerhof (PBE) exchange−correlation functional.[61] The projector augmented-wave (PAW) method of Blöchl[62−64] was used to represent atomic cores with the VASP "PBE O 08Apr2002" PAW used for oxygen and the VASP "PBE H 15Jun2001" PAW used for hydrogen. The settings "PREC = accurate" and "ENCUT = 800.0" were used for all calculations. The dipole interactions between periodically repeated cells were cancelled in the z-direction, which was the direction of applied electric fields. Fermi smearing with a 300 K electronic temperature was used to calculate the occupations of the Kohn-Sham states. Ab initio molecular dynamics calculations used a 0.8 fs time step. The microcanonical ensemble (NVE) was used for simulations of two well-separated waters in a large box (Section III.I), while a canonical ensemble (NVT) using the algorithm of Nosé[65,66] at T = 300 K and the VASP default Nosé-mass corresponding to 40 MD time steps (32 fs) was used to generate snapshots of a water slab (Section III.IV), which were then used to calculate the change in charge and potential when a field was applied. Our systems were large for DFT calculations, and we do not expect much band dispersion for a molecular liquid such as water, so Brillouin-zone sampling was accomplished using the Baldereschi mean value point.[67]

II.VI. Quantum Chemistry. To benchmark the dissociation curve of a single water molecule in the presence of an electric field (Section III.III), we performed unrestricted Hartree−Fock (UHF) calculations in open boundary conditions using the Psi4 code[68] with a Dunning cc-pCVTZ basis set.[69] Electric fields were treated by including a $-\hat{\mathbf{p}}\cdot\mathbf{E}$ term in the one-body Hamiltonian, where $\hat{\mathbf{p}}$ is the dipole operator and $\mathbf{E}$ is the electric field. For all field strengths considered, we started by placing the dissociated H atom at a hydrogen−hydroxyl distance, r_{H-OH} (see Figure 4a), of 0.94 Å. Converging this at the UHF level, we then sequentially increased the r_{H-OH} distance, using the previous step's wave function as the starting guess for the state at the new position. This was repeated until the dissociation limit and then redone in reverse. The lowest energy states at each r_{H-OH} separation were identified using this procedure, after which the observables were computed. In particular, the total charge on the disassociated hydrogen atom was computed using the distributed multipole analysis method.[70] Charges within 0.614 and 1.228 Å were associated with the hydrogen and oxygen atoms, respectively. This is not expected to be quantitatively rigorous for small r_{H-OH} distances where the charge cannot be unambiguously associated with specific atoms, but for dissociation, this should be appropriate. While this procedure does not produce the correct wave function spin symmetry, a proper broken symmetry state dramatically improves the dissociation curve and charge distribution over single-reference restricted calculations, which is especially important for dissociation problems.

III. RESULTS

III.I. Two Water Molecules in an Electric Field. We first perform a simple example to illustrate the differences between the QEq and ACKS2 charge distribution methods in the presence of an electric field. Here, we simulate two water

https://doi.org/10.1021/acs.jctc.1c00975
J. Chem. Theory Comput. 2022, 18, 580−594

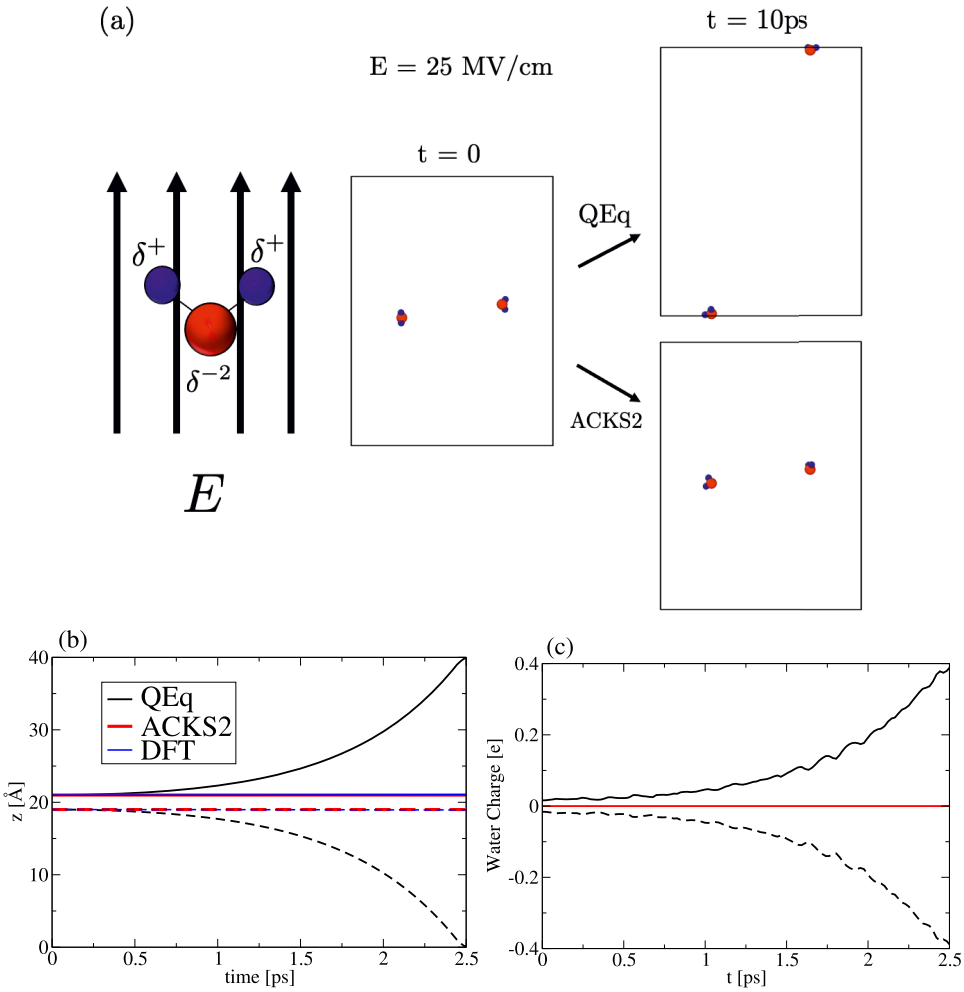

Figure 1. (a) Visualization of two water molecules at $t = 0$ and 10 ps when an electric field ($E = 25$ MV/cm) is applied in the positive z-direction. QEq predicts the water molecules move to the top and bottom of the box while ACKS2 shows no translation of the water molecules. These simulations were run for 100 ps, and the water molecule positions do not change after ≈2.5 ps. (b) The z-position versus time and (c) water charge versus time for both water molecules using QEq (black), ACKS2 (red), and DFT (blue) with $E = 25$ MV/cm. One water molecule is denoted by the solid line and the other is denoted by the dashed line. Note that the DFT results overlap with the ACKS2 results in panel (b) and both ACKS2 water molecules overlap in panel (c). We do not include the DFT results in panel (c) since the results in panel (b) indicate that the waters are not accumulating a net charge, as is the case in QEq.

molecules separated by a distance sufficiently large that they should be considered noninteracting. The simulations are run with a box size of $Lx = Ly = 30$ Å and $Lz = 40$ Å unless otherwise noted. The molecules were initially separated by 21.28 Å, intentionally greater than a Coulomb cutoff of 10 Å. Additionally, we offset the molecules by 2.0 Å in the z-direction. The simulations are run in an NVE ensemble.

Figure 1a shows a visualization of the water molecules when $E = 25$ MV/cm for both QEq and ACKS2. Figure 1b,c shows the charge on each molecular water and the associated z-position within the box for both QEq and ACKS2. When using QEq, the water molecules accumulate a nonzero net charge and move to the top and bottom of the box in a manner that mirrors the water's charge. However, when using ACKS2, we observe that the water molecules remain charge neutral and do not translate due to the applied electric field. The ACKS2 behavior coincides with the DFT result where the two water molecules do not translate. The QEq and ACKS2 simulations were run out to 100 ps, and the behavior remains constant after ≈2.5 ps. Note that the ionization energy of molecular water is 12.621 ± 0.002 eV,[71] while the electron affinity of molecular water is zero or very small.[72,73] Therefore, charge transfer between two isolated water molecules should not be energetically favored unless there is a potential difference of more than 12.6 V between the molecules, which would correspond to an along-field separation of more than 50 Å in a 25 MV/cm electric field. This suggests that in the case of two water molecules separated by a relatively large distance under an externally applied electric field, we observe unphysical charge transfer using QEq, while we observe the physically correct charge transfer with ACKS2.

The functional form of the electric field shown in eq 4 has spatial dependence. Since one molecule is at a greater z_i, the electrostatic energy of a net charge located on a water is different between the two waters. Since QEq allows for global charge transfer between the two waters, this results in the water with the greater z_i to have a net positive charge and the water with the lesser z_i to have a net negative charge. ACKS2 prevents this charge-transfer behavior because the waters are separated by a relatively large distance.

To further demonstrate the charge distribution using QEq and ACKS2, we now run nondynamic calculations with the waters at fixed z-positions z_1 and z_2. Specifically, in each

https://doi.org/10.1021/acs.jctc.1c00975
J. Chem. Theory Comput. 2022, 18, 580−594

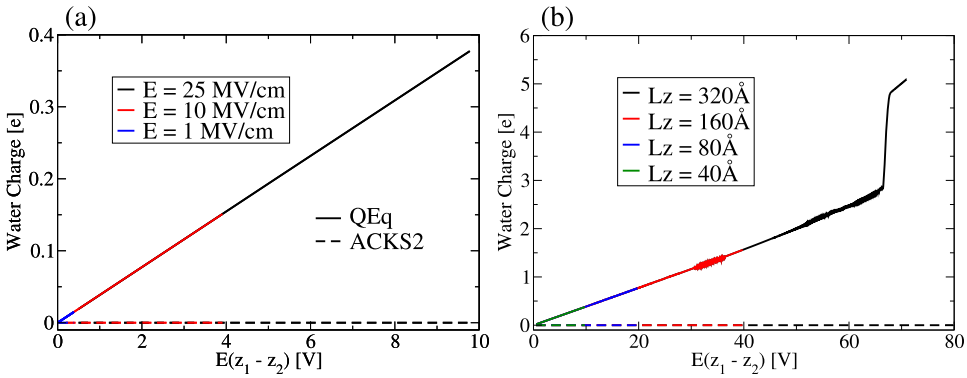

Figure 2. Water charge versus the applied electric potential between the two waters, $E(z_1 - z_2)$, for (a) varying electric field strengths and (b) different box sizes using QEq (solid) and ACKS2 (dashed). In panel (a), E = 25 MV/cm (black), 10 MV/cm (red), and 1 MV/cm (blue). For each electric field strength, the lines fall exactly on top of one another, though with increasing electric field, the maximum electric field potential increases. In panel (b), E = 25 MV/cm with Lz = 320 Å (black), 160 Å (red), 80 Å (blue), and 40 Å (green). Similar to panel (a), the lines fall exactly on top of one another, up to the maximum electric field potential dictated by the size of the box. Only the charge of the "top" water is shown to more clearly illustrate the trends.

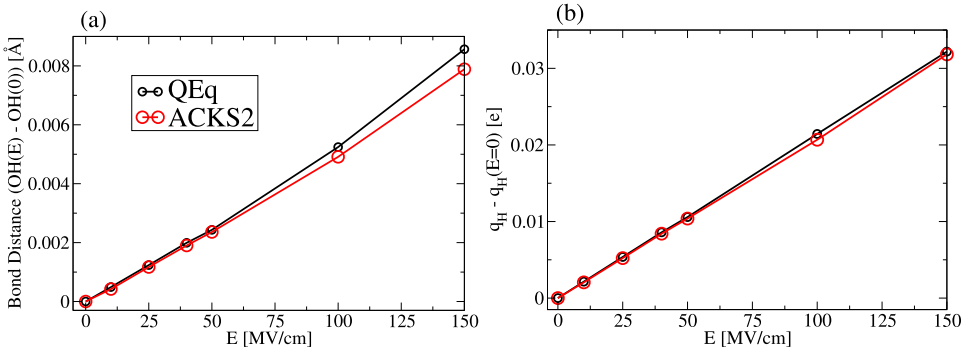

Figure 3. (a) Oxygen−hydrogen bond distance and (b) hydrogen charge as a function of electric field strength using QEq (black) and ACKS2 (red). The y-axis in both plots is shifted by the zero-field result to provide a more direct comparison of the electric field effect between the two charge distribution methods.

calculation, we fix the position of the oxygen and allow the hydrogens to relax. We use the same x- and y-coordinates for the oxygens as in Figure 1. Figure 2 shows the net charge on the "top" water as a function of the applied electric potential between the two waters, $E(z_1 - z_2)$. Figure 2a varies the strength of the electric field at a constant box size of Lz = 40 Å, while Figure 2b varies the box size at a constant electric field strength of 25 MV/cm. For a given charge distribution method, the lines fall exactly on top of one another up to the maximum electric field potential difference dictated by the electric field strength and the maximum z-separation of the two waters. This is except for the black curve in Figure 2b. In this case, when the applied electric potential exceeds ≈66.5 V, the charges on the hydrogens and oxygen of the top water are all positive, and the charges on the hydrogens and oxygen of the bottom water are all negative. At this point, the Coulomb interactions are strong enough to exceed the bonding interactions and the hydrogens dissociate from the oxygen. Without the bonded hydrogens, the oxygen sees a rapid jump in its charge that reflects the jump in charge shown in the black curve of Figure 2b.

Figure 2 demonstrates several key points. First, the water molecules remain charge neutral with ACKS2 over the entire range of electric field strengths, distances between atoms, and box sizes that we investigated. Second, the global charge transfer inherent in QEq results in a non-neutral net charge on each water molecule that is a linear function of the difference in electric potential between the two waters. We note that the slope of the QEq lines in Figure 2a,b is dictated by the electronegativity and the atomic hardness of the oxygen and hydrogen atoms as well as the intramolecular Coulomb interactions. For this QEq force field, the slope in Figure 2a,b is 0.0386 e/V, neglecting the data where $E(z_1 - z_2)$ exceeds ≈66.5 V.

The large ionization energy and zero (or very small) electron affinity of an isolated molecular water are discussed above. In principle, it would be energetically favorable for an isolated water molecule to lose an electron if the potential difference between the water molecule and some other point in space exceeds the ionization energy. However, even for very strong electric fields such as 25 MV/cm, the water molecule and such a point in space would be separated by a large distance, e.g., more than 50 Å at 25 MV/cm, and the probability of an electron tunneling through the relevant barrier would be negligible. Coordination to other molecules, an intervening dielectric medium, and high temperatures all increase the probability of such an event, and for solvated ions, long-ranged charge transfer becomes commonplace. One of the core issues with standard charge distribution methods is that they cannot handle such phenomena, with ACKS2 preventing any long-ranged charge transfer, while QEq misses the discreet nature of real charge-transfer processes. It is theoretically possible to accurately capture such processes in a more advanced formulation like the coarse-grained electron model (C-GeM)[74,75] or the explicit electron ReaxFF (eReaxFF) model.[76] In any case, a water

https://doi.org/10.1021/acs.jctc.1c00975
J. Chem. Theory Comput. 2022, 18, 580−594

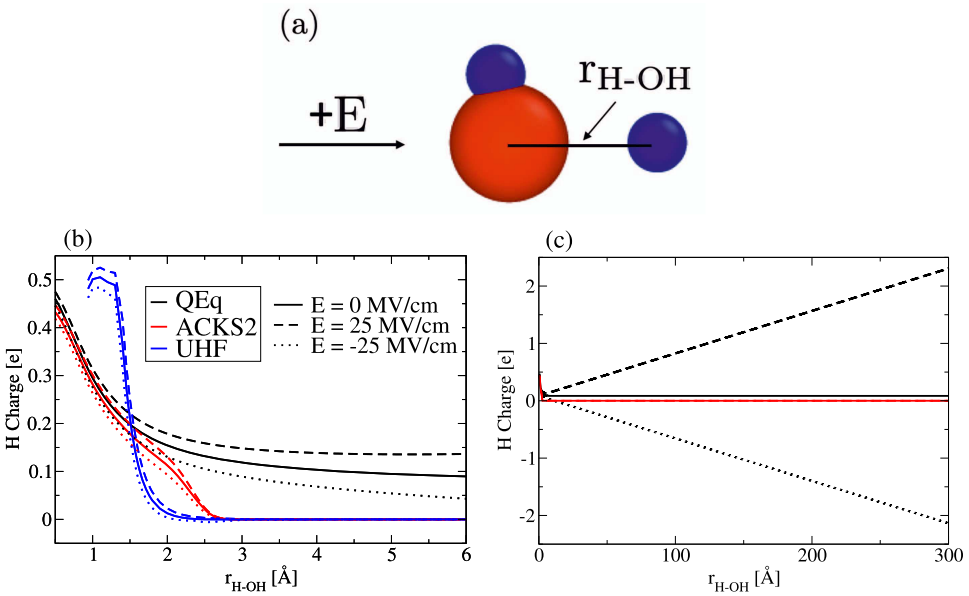

Figure 4. (a) Visualization of a single dissociating water in an electric field. (b) Short-range and (c) long-range behaviors of the dissociating hydrogen charge as a function of hydrogen−hydroxyl distance, r_{H-OH}, using (black) QEq, (red) ACKS2, and (blue) UHF. The solid, dashed, and dotted lines represent $E = 0$, +25, and −25 MV/cm, respectively. Both plots show the same data but focus on varying distances to highlight the effect of the electric fields with the different methods. The right plot only includes the QEq and ACKS2 results where it is implied that the UHF method predicts a 0 charge at distances greater than ≈2.5 Å.

accumulating multiple extra electrons, as indicated in Figure 2b, is simply an unphysical result.

III.II. Single Molecular Water in an Electric Field. To further compare QEq versus ACKS2 in an external electric field, we next look at a single molecular water. In these simulations, we once again use an NVE ensemble. Figure 3 shows the oxygen−hydrogen bond distance and the hydrogen charge as a function of electric field strength using both QEq and ACKS2. In each of these plots, the *y*-axis is plotted as the difference between the results at a given electric field strength and the zero-field result. This allows us to compare the electric field response more closely between QEq and ACKS2. Both QEq and ACKS2 predict increases in the oxygen−hydrogen bond distance and the hydrogen charge as a function of electric field strength and show minimal quantitative differences. Even at an electric field strength of 150 MV/cm, the oxygen−hydrogen bond distance changes by 0.0086 Å in QEq and 0.0079 Å in ACKS2 for less than a 0.001 Å difference between the two methods. Similarly, at an electric field strength of 150 MV/cm, the hydrogen charge changes by 0.0322 *e* in QEq and 0.0318 *e* in ACKS2. In both QEq and ACKS2, the water molecule remains electroneutral and does not translate. These results show that the electronic polarization response of a water molecule in an electric field is very similar in QEq and ACKS2. Since capturing such a polarization response is one of the main reasons to use a charge distribution method, these results show that both QEq and ACKS2 can accomplish this goal. However, while this might be true for a single water molecule, the electronic response would be very different for large molecules such as a peptide or polymer.

The primary difference in comparing the single molecular water results to the two molecular water results in the previous section is the length scale in which charge transfer can occur. The two water molecule system demonstrated a prominent shortcoming of QEq in that the water molecules can exchange charges over large distances resulting in unexpected behavior, while the framework of ACKS2 prevents this long-range charge transfer and produces more physical results. In the case of a single molecular water, charge transfer can only occur intramolecularly, which is on the order of 1 Å, and therefore, we do not see prominent quantitative differences between QEq and ACKS2.

III.III. Single Dissociated Water in an Electric Field. One of the appealing attributes of ReaxFF in comparison to nonreactive molecular dynamics methods is its ability to capture phenomena such as dissociation. In this setup, we use a single water molecule, where we fix the position of the oxygen and place one of the hydrogens at varying distances r_{H-OH} from the oxygen. At each r_{H-OH} distance, the second hydrogen that is bonded to the oxygen is allowed to relax. This is shown schematically in Figure 4a. This setup effectively models the dissociation of a water into a hydroxyl and a hydrogen. In reference to Figure 4a, we then ran two additional sets of calculations with $E = -25$ and +25 MV/cm. Figure 4b,c shows the charge on the dissociating hydrogen as a function of r_{H-OH}. For each of these tests, we run QEq and ACKS2 and provide a reference quantum chemistry result using the Psi4 framework at the unrestricted Hartree−Fock (UHF) level. Bond breaking is a notoriously difficult problem for quantum chemistry methods, but previous work has shown that UHF is quite accurate for water dissociation and gives qualitatively correct behavior throughout the dissociation curve.[77]

UHF predicts the hydrogen to have a negligible charge beyond $r_{H-OH} \approx 2.5$ Å. At shorter distances, a positive electric field slightly increases the hydrogen charge, while a negative electric field slightly decreases the hydrogen charge, as would be expected based on simple electrostatic interactions. The experimentally measured ionization energy of H is 13.598 eV,[78] while the experimentally measured electron affinity of OH is only 1.828 eV;[72] thus, there is no doubt that H_2O should dissociate to neutral H and OH in vacuum. However, even many types of DFT calculations give spurious partial charges when

https://doi.org/10.1021/acs.jctc.1c00975
J. Chem. Theory Comput. 2022, 18, 580−594

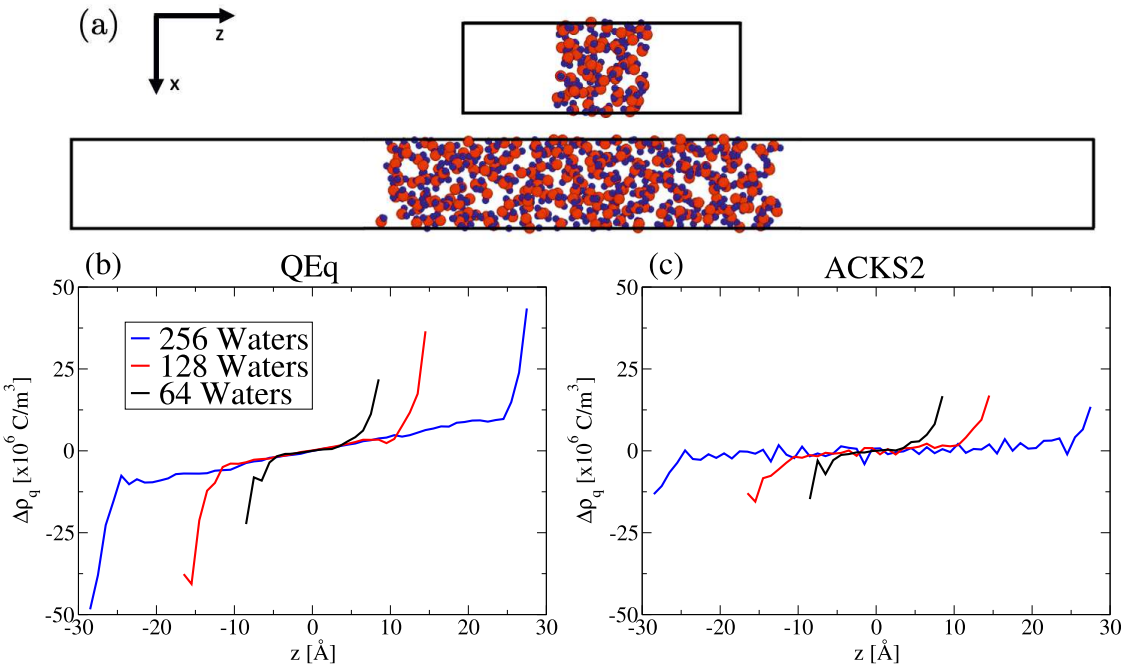

Figure 5. (a) Visualization of two slab configurations where the top configuration has 64-waters, while the bottom configuration has 256-waters. The size of the total vacuum is approximately twice the size of water slab. The difference in charge density, ρ_q, between E = 10 and 0 MV/cm as a function of z-position using (b) QEq and (c) ACKS2 for the 64-water slab (black), 128-water slab (red), and 256-water slab (blue). The data is averaged over the x- and y-positions using z-bins of 1 Å. In all cases, the center of the slab is shifted so that it sits at z = 0.

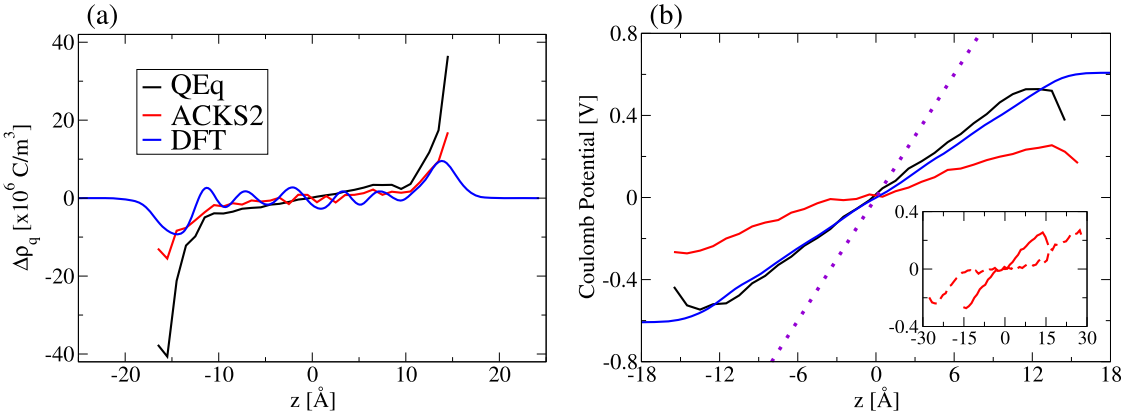

Figure 6. (a) Difference in charge density, ρ_q, between E = 10 and 0 MV/cm and (b) the corresponding difference in the Coulomb potential as a function of the z-position using QEq (black), ACKS2 (red), and DFT (blue) for the 128-water slab. The purple dotted line shows the negative of the applied potential. The inset in panel (b) shows the ACKS2 data for the 256-water slab (dashed) to emphasize the plateau in the middle of the slab. The ReaxFF data is averaged over the x- and y-positions using z-bins of 1 Å. The DFT data is averaged over the x- and y-positions and over six snapshots separated by ∼1 ps of dynamics between each snapshot. The DFT data is further convoluted with a Gaussian filter with a standard deviation of 1 Å to reduce the high-frequency noise. In panel (b), the ReaxFF curves are generated by summing over j for the Coulomb term in eq 2 for each atom i. In all cases, the center of the slab is shifted so that it sits at z = 0.

dissociation results in open-shell products such as H and OH. Therefore, we compare our results to UHF instead of DFT in this case. In the case of ACKS2, the main qualitative features of the quantum chemistry result are reproduced. Although the hydrogen charge exhibits a somewhat different shape at short r_{H-OH} distances, we note that the partial charge partitioning at bonding distances is not a unique quantity. We used the Gaussian distributed multipole analysis (GDMA) protocol[70] here, but other choices would result in slightly different results. In contrast, QEq does not predict a 0 charge at large distances, similar to results that have been reported previously in the original QTPIE paper[13] and in the context of hydrogen fluoride dissociating within the original ACKS2 paper.[14] Figure 4c displays the most notable result with the long-range behavior in an applied electric field. This is another situation where the global charge transfer inherent in QEq and the implementation of the electric field into ReaxFF via eq 4 produce unphysical results. In the case of a positive electric field, the hydrogen charge continually increases with r_{H-OH} and can exceed values of +1 e, which is clearly unphysical. Correspondingly, in the case of a negative electric field, the hydrogen charge continually decreases with r_{H-OH}, reaching values of −2 e and beyond. These results indicate that there are inherent issues in treating dissociation with QEq, particularly with an electric field. ACKS2

https://doi.org/10.1021/acs.jctc.1c00975
J. Chem. Theory Comput. 2022, 18, 580−594

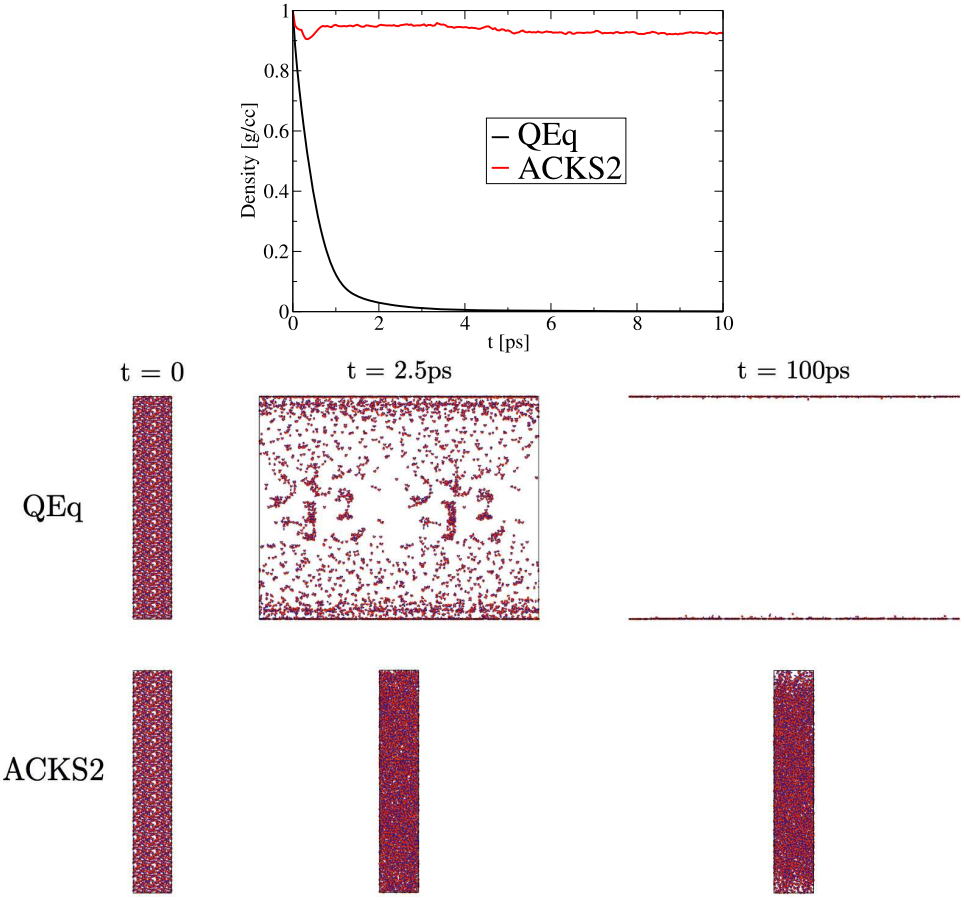

Figure 7. (a) Density versus time using QEq (black) and ACKS2 (red) with NPT simulations with Lz = 16 nm and E = 25 MV/cm. These simulations were run out to t = 100 ps but only the first 10 ps are shown to illustrate the early time behavior most clearly. (b) Visualizations of the NPT simulations at t = 0, 2.5, and 100 ps for both QEq and ACKS2. Only a small subsection of the QEq simulations at t = 100 ps is shown. Note that at t = 0, 2.5, 10, and 100 ps, the corresponding box areas for the QEq simulations are A = 7.66, 414.23, 6505.72, and 23 059.76 nm^2, respectively. At t = 0, 2.5, 10, and 100 ps, the corresponding box areas for the ACKS2 simulations are A = 7.66, 8.05, 8.29, and 8.15 nm^2, respectively.

offers a more reasonable description at long ranges. The short-range behavior of ACKS2 could be tuned to match the quantum chemistry more closely with a reparameterization against the quantum data.

III.IV. NVT Simulations of Water Slab in an Electric Field. We next turn our attention to bulk water systems in an electric field using the canonical ensemble (NVT), where we generated water slabs with varying amounts of water. First, we equilibrated a bulk sample of 64 waters using the isothermal–isobaric ensemble (NPT) with T = 300 K and P = 1 atm for 1 ns. The Nosé–Hoover thermostat and barostat used a damping constant of 50 and 500 fs, respectively. Periodic boundary conditions were used in all directions. Next, we ran an NVT simulation at T = 300 K with periodic boundary conditions in the x- and y-directions and a fixed boundary condition in the z-direction for 100 ps. Prior to running the NVT simulation, the box was carefully shifted so that no waters were crossing the z-boundary. To produce larger slabs of water, we replicated the system 2 and 4 times in the z-direction so that we had systems with 128 and 256 waters, respectively. Next, for each slab, we shifted the z-boundaries so that there was a 1 slab length of vacuum above and below the water slab. Finally, we then ran another NVT simulation for 100 ps to allow the interface to relax. Figure 5a shows the 64- and 256-water slabs that were generated in this manner.

Figure 5b,c shows the difference in charge density between E = 10 and 0 MV/cm (i.e., $\rho_q[E = 10\ \text{MV/cm}] - \rho_q[E = 0]$, where ρ_q is the charge density) as a function of z_i using both QEq (Figure 5b) and ACKS2 (Figure 5c). Note that the atom positions were kept fixed when the field was applied, so we are only investigating the electronic response to the field, as captured by the charge distribution model in QEq and ACKS2. The contribution to the dielectric response from reorientation of the permanent dipoles of water in the field is absent, and therefore, these results should be compared to the behavior of water at optical frequencies where the permanent dipole moments are unable to reorient. Figure 5c (ACKS2) shows a qualitatively correct charge distribution for a slab of polarizable material in an electric field. To confirm this behavior, Figure 6a compares the results for the 128-water slab to a DFT calculation. We note that a charge is associated with each atom in QEq and ACKS2, while the charge is resolved on a fine grid of points in DFT. Therefore, DFT reveals considerable structures in the change in charge density when a field is applied to a given snapshot of atomic positions that is not apparent in QEq or ACKS2. Due to translational invariance of the time-averaged bulk water structure, this structure slowly averages out in the center of a sufficiently thick slab, but this is not true near the surfaces of the slab. The induced dipoles create oppositely signed layers of charge at each surface, but the charges associated with the induced dipoles on each side of a point in the interior of

https://doi.org/10.1021/acs.jctc.1c00975
J. Chem. Theory Comput. 2022, 18, 580–594

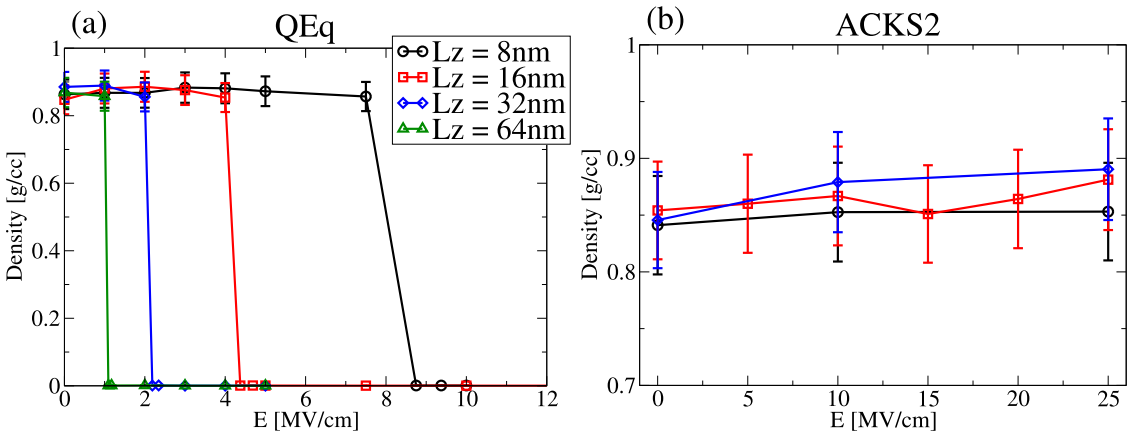

Figure 8. Density versus electric field strength using (a) QEq and (b) ACKS2 with NPT simulations with varying *Lz*. *Lz* = 8 nm (black), 16 nm (red), 32 nm (blue), and 64 nm (green). *Lz* = 64 nm with ACKS2 was not run as the density for the smaller *Lz* values all fall within the error bar indicating that the density is not changing with box size. The error bars correspond to the standard deviation in the density for the last 20 ps of the 100 ps simulation.

the slab cancel out leading to a zero average charge density throughout the middle of the slab. In contrast, Figure 5b (QEq) shows a charge density that varies linearly with z_i, and hence with the applied electric potential, superimposed on top of the surface charge layers due to the induced dipoles. This linearly varying charge density is similar to the linearly varying charge density that we observed for two water molecules in an electric field, and it indicates long-ranged charge transfer from the molecules on one side of the slab to the water molecules on the other side of the slab.

Long-ranged charge transfer of this type is unphysical in an insulator such as water. Water has a band gap of ≈7 eV, and we would not expect charge transfer until the potential difference across the water is at least equal to the band gap. The incorrect charge distribution obtained from QEq is a result of reinforcing errors due to the two main approximations in QEq (discussed in Section II.II). The metal-like charge transfer allows charge to transfer long distances in response to small differences in potential, while the short-ranged Coulomb interactions prevent the induced charge from fully screening the applied field, as would occur in a real metal. The absence of complete screening in QEq is demonstrated in Figure 6b. Note that this figure shows the induced potentials, i.e., it does not include the applied potential. The purple dotted line in Figure 6b shows the applied potential with the sign reversed for easy comparison to the induced potential. The results for both QEq and DFT show partial screening of the applied field, corresponding to a relative permittivity of $\epsilon_{r,QEq} = 1.79$ and $\epsilon_{r,DFT} = 1.72$ in good agreement with the experimental relative permittivity of water at optical frequencies $\epsilon_r = 1.78$. The dielectric-like screening of an applied potential in QEq is an example of cancellation of the errors due to the main approximations in QEq. Due to the metal-like charge transfer, the charge density is proportional to the applied potential throughout the middle of the slab, but the potential only sees the nearby charge due to the short-ranged Coulomb interactions, and thus the gradient in the charge density produces a screening potential that agrees well with the experiment. In contrast, the induced potential in ACKS2 is smaller and goes to zero in the middle of a thick slab, an effect that is just beginning to be apparent for the 128-water slab, but becomes dramatically apparent in thicker slabs (see the inset in Figure 6b). ACKS2 fixes the metal-like charge transfer of QEq, but the short-ranged Coulomb interactions prevent the layers of charge at the surfaces from screening the middle of a thick slab.

These results show that QEq gives surprisingly accurate electronic screening properties for an applied electric field: i.e., for fixed atomic positions. In contrast, ACKS2 gives qualitatively accurate charge distributions, but they fail to screen an applied field in the center of a thick slab due to the use of short-ranged Coulomb interactions. Although the charge distribution properties of ACKS2 are obtained via an atom-in-molecule derivation from Kohn-Sham DFT and inherently restricts charge transfer past an atom-type-dependent cutoff distance, the use of short-ranged Coulomb interactions is not derived from DFT and is physically incorrect for an insulator such as water. Two sheets of charge, such as those that occur at the surfaces of a polarizable medium in an electric field, produce an electric field that is independent of the thickness of the medium. This infinite range effect cannot be captured by short-ranged Coulomb interactions. Therefore, once the extent of a system in the field direction becomes larger than the cutoff for the Coulomb interactions, an accurate charge distribution will result in inaccuracies in the screening of the electric field and an accurate electric field screening will result in inaccuracies in the charge distribution. Next, we will investigate the consequences of these charge distribution and potential screening results for the dynamics of a water slab.

III.V. NPT Simulations of Bulk Water in an Electric Field. We now explore the differences in the charge distribution methods through bulk water systems in an electric field using NPT simulations. In all cases, $T = 300$ K and $Pxx = Pyy = 1$ atm. The *z*-direction remains fixed, while the *x*- and *y*-directions are allowed to vary. The Nosé−Hoover thermostat and barostat use a damping constant of 50 and 500 fs, respectively. Figure 7 shows qualitative differences in the overall density as a function of time when comparing QEq to ACKS2. In this case, *Lz* = 16 nm and *E* = 25 MV/cm. We see that for this set of parameters, the QEq density reaches nearly 0 after ≈4 ps while ACKS2 converges to a density of about 0.87 g/cc. With QEq, the water rapidly moves to the top and the bottom of the box. The species at the top and bottom of the box accumulate a positive and negative charge, respectively, similar behavior to what is observed in Figures 1 and 2 with regard to the two molecular water results. Due to this accumulation of charge, the species are spaced out at the top and bottom surfaces and result in the large area seen over time and effectively 0 density.

Figure 8 shows how the density changes as a function of electric field strength with varying box sizes. With QEq, we see

https://doi.org/10.1021/acs.jctc.1c00975
J. Chem. Theory Comput. 2022, 18, 580−594

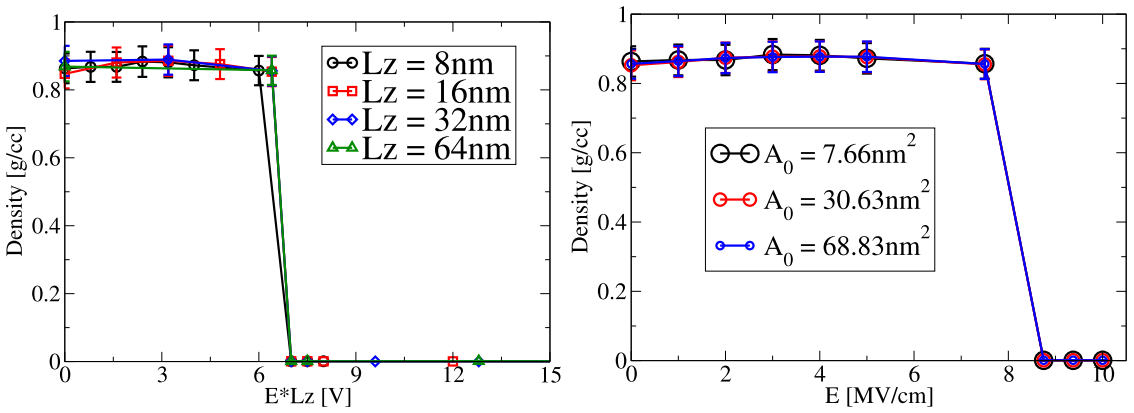

Figure 9. (a) Density versus electric field strength multiplied by the box size in the z-direction using QEq with NPT simulations. This shows the same data as Figure 8a but using a different x-axis. This x-axis shows that the QEq data collapses and the primary quantity of interest is $E \times Lz$. Lz = 8 nm (black), 16 nm (red), 32 nm (blue), and 64 nm (green). (b) Density versus electric field strength for varying simulation areas. Here, Lz = 16 nm in all cases. The initial area of the box, A_0 ($Lx_0 \times Ly_0$), A_0 = 7.66 nm^2 (black), 30.63 nm^2 (red), and 68.93 nm^2 (blue). Since Lz is constant, each curve also represents a different number of water molecules.

that the density remains at ≈0.87 g/cc until a critical electric field strength and the density goes to ≈0. Note that the density reported in this section of ≈0.87 g/cc for both QEq and ACKS2 is slightly less than the bulk density of ≈0.92 g/cc due to the hard walls in the z-direction. Furthermore, the value of this critical electric field strength changes as a function of box size, with the critical electric field strength decreasing with increasing box size. With ACKS2, we see that the density is not a function of box size as the density for each box size is the same for a given electric field strength within the error bars. We note once more that we are not indicating that ACKS2 is providing a completely accurate description of the water density as a function of electric field strength but rather that the density converges as a function of box size.

When using QEq with an electric field, it is evident that properties do not converge as a function of box size if long-range charge transfer can occur. Figure 9a shows that the NPT data from Figure 8a collapses when the x-axis is reframed as the quantity $E \times Lz$. Figure 9b elucidates that the key quantity is the size of the box in the direction of the field rather than the dimensions perpendicular to the field or the total number of molecules in the system. Specifically, in Figure 9b, Lz is held constant at Lz = 16 nm while the initial area perpendicular to the field, A_0, is changed. For each A_0, the same density is predicted at a given electric field strength. Figure 9 demonstrates that the primary quantity of interest in QEq when using an electric field is not the electric field, but the potential drop, i.e., the product of the electric field and size of the box in the direction of the electric field.

Our simulations with two water molecules showed that QEq allows unphysical charge transfer within a system that has two parts, and this results in the two parts being pulled apart along the electric field direction. Our results for a slab of water with QEq show that even a system that is initially a single connected region of liquid water can be pulled apart leading to two separated regions of liquid with vapor in between. This suggests that an electric field represented with QEq is inducing a negative pressure in the slab of water, which at some point leads to the separation of the water into liquid and vapor components.

We can estimate the pressure within the slab as follows: consider a slab of water extending from $-L/2$ to $L/2$ in the z-direction with applied potential $V(z) = -Ez$. In Figure 5b, we observed a linear relationship between the average net charge density $\rho(z)$ at position z within a water slab and the applied potential using QEq. In particular

$$\rho(z) = -\overline{\eta}^{-1} V(z) \tag{5}$$

where $\overline{\eta}$ is a fitting parameter characterizing the observed linear relationship shown in Figure 5a. Fitting the results in Figure 5b, we obtain $\overline{\eta} = 4.63 \times 10^{-9}$ V m^3/C = 4.63 V^2/GPa. Note that Figure 5b is calculated with static atomic positions, and therefore, the value of $\overline{\eta}$ obtained from it does not include any effects from the reorientation of the permanent dipole moments of the waters in the applied field. There are two reasons that the use of such a result is reasonable: (a) the reorientation of the dipole moments in water is relatively slow, as demonstrated by the frequency-dependent dielectric constant of water. The effect of reorienting dipole moments on the dielectric constant is relatively small for the subpicosecond time scales, where we see our water slabs break apart in our computational experiments. (b) The short-range electrostatics in the QEq model should prevent the reorientation of the dipole moments from having an effect within the middle of a water slab that is much thicker than the electrostatic cutoff. Just like the induced dipoles, the net effect of reorientation of the permanent dipoles is to introduce layers of charge at the surfaces of the slab. The short-ranged electrostatics should prevent the effects of these charge layers from reaching the interior of a thick slab. Therefore, we feel justified in using the $\overline{\eta}$ obtained from Figure 5b in our estimate of the pressure induced by an applied electric field.

In Figure 6b, we also observe a linear relationship between the screened potential $\tilde{V}(z)$ and the applied potential $V(z)$ within the middle of a water slab represented with QEq. We obtain a relative permittivity of ϵ_r = 1.79 for QEq by fitting the data in Figure 6b. Thus, the screened electric field $\tilde{E} = \epsilon_r^{-1} E$. The screened electric field produces a force dF on the charge induced in an infinitesimal volume dΩ

$$\frac{dF}{d\Omega} = \tilde{E}\rho(z) = \epsilon_r^{-1} E \overline{\eta}^{-1} Ez = \epsilon_r^{-1} \overline{\eta}^{-1} E^2 z \tag{6}$$

and if the system is to remain in quasi-static equilibrium, this force must be balanced by a gradient in the pressure

$$\frac{dP}{dz} = \frac{dF}{d\Omega} = \epsilon_r^{-1} \overline{\eta}^{-1} E^2 z \tag{7}$$

https://doi.org/10.1021/acs.jctc.1c00975
J. Chem. Theory Comput. 2022, 18, 580−594

We then integrate to get

$$P(z) = P(0) + \frac{1}{2\epsilon_r \bar{\eta}} E^2 z^2 \tag{8}$$

The value of $P(0)$ will depend on the boundary conditions that we apply to our slab. Consider boundary conditions corresponding to our NPT simulations above, i.e., a hard wall is applied along the surfaces of the slab at $z = \pm L/2$, and periodic boundary conditions with barostats are applied in the x- and y-directions. The average pressure in the x- and y-directions is

$$\bar{P} = \frac{1}{L}\int_{-L/2}^{L/2} P(z)\, dz = P(0) + \frac{1}{24\epsilon_r \bar{\eta}} E^2 L^2 \tag{9}$$

The barostats enforce $\bar{P} = 0$, which implies

$$P(0) = -\frac{1}{24\epsilon_r \bar{\eta}} E^2 L^2 \tag{10}$$

Note that the pressure induced by the applied field is negative (i.e., the field pulls the slab outwards putting the slab under tension), and in the thermodynamic limit, it is always energetically favorable for a liquid to break into regions of liquid and vapor rather than sustain a negative pressure. However, for values of pressure that are less negative than the spinodal pressure P_s, regions of vapor must nucleate and grow, and this usually only occurs for large or long MD simulations. However, once the pressure reaches the spinodal pressure, nucleation is no longer necessary, and the system can break into small regions of liquid and vapor within the time scale of a few intermolecular vibrations. There is considerable disagreement about the spinodal pressure for water, but values range from around −50 to −200 MPa with experimental results typically on the lower end and theoretical values on the higher end.[79] Taking a geometrical mean value of $P_s = -100$ MPa, we can estimate the maximum potential drop that can be sustained across a slab of water treated with QEq before the center of the slab breaks into liquid and vapor by setting $P(0) = P_s$. Solving gives a maximum potential drop of $EL = \sqrt{24\epsilon_r \bar{\eta} P_s} = 4.5$ V. Given the uncertainties in our estimate (e.g., the value for the spinodal pressure of water), this value is in good agreement with the observed rapid decrease in density at a potential drop of $EL = 6$–7 V demonstrated for several different field strengths in Figure 9a. Notably, if we allowed a small screening contribution from reorientation of the permanent dipoles of water despite the consideration discussed above, it would increase both ϵ_r and $\bar{\eta}$, which could easily explain the difference between our estimate and the results of our computational experiments.

The agreement between our estimate and the data shown in Figure 9a affirms that there is a negative pressure that ultimately separates the water slab using QEq with an applied electric field. The result of our estimate follows from eq 5, which describes the linear relationship of the applied potential and the net charge density. As we see in Figure 5c, the observed plateau around 0 for the net charge density using ACKS2 infers an infinite (or very large) $\bar{\eta}$. From eq 10, this indicates that EL is infinite (or very large) before the water separation would occur when using ACKS2.

The derivation suggests that the unphysical charge distribution that results from the global charge transfer using QEq under an externally applied electric field (seen in Figure 5b) results in catastrophic physics beyond an electric potential threshold (seen in Figures 7, 8a, and 9a). Physically, beyond this electric potential threshold, the electric field exerts a force on the atomic charges that exceed the bonding forces, keeping the system in a bonded state. In principle, this catastrophic behavior is not true solely for water but would hold true for any material if the potential drop was large enough. The nonglobal charge transfer within ACKS2 addresses this core issue.

IV. CONCLUSIONS

In this paper, we have compared the QEq and ACKS2 charge distribution methods for water in the presence of an external electric field. Here, we implement the electric field as is commonly done in ReaxFF simulations by introducing the electric field potential into the electrostatic energy. In charge distribution models, this is necessary to allow the system to form an internal electric field that opposes the external electric field.

We have shown that in this context the presence of an electric field amplifies the nonphysical long-range charge transfer in QEq. In QEq, since the charge distribution is dependent on the electric potential between molecules, we observe that the charge distribution does not converge and becomes increasingly inaccurate as a function of system size. We see that there is a potential threshold where the force from the electric field overcomes the bonded forces between the water molecules causing the liquid water to split and move up or down the box with respect to the direction of the applied field. The potential threshold is dependent on the strength of the bonding forces in the system. We see that in the case of two water molecules separated by a relatively large distance where there is no intermolecular bonding force, any potential difference between the waters causes the waters to accumulate a net charge, which leads to the water molecules moving up or down the box. For a hydrogen-bonded water slab confined between two hard walls, the potential threshold is ≈6–7 V. While in this paper we have focused solely on water, this potential threshold would arise in any material using QEq with an external electric field, as formulated by Chen and Martínez.[16] We note that an alternative formalism that uses the relative distance between atom-neighbor pairs in an effective atomic electronegativity[34−36] may help ameliorate some of the artifacts seen for QEq with electric fields in this work.

In general, we find that ACKS2 due to its nonglobal charge transfer addresses the major issues with applying QEq in an external electric field. We observe that ACKS2 under an external electric field predicts neutral charges on water molecules separated by large distances and neutral charges on a dissociated hydrogen and hydroxyl molecule, as one would expect based on experimental results for ionization energies and electron affinities, as well as DFT and quantum chemistry calculations. Furthermore, as we increase the size of our bulk systems, the charge distribution and the water density converge to bulk values in the center of the slab away from any interface or hard wall. However, we find that in ACKS2 the combination of nonglobal charge transfer and short-ranged Coulomb interactions result in inaccurate electronic screening properties. Interestingly, QEq gives surprisingly accurate electronic screening properties due to the cancellation of effects between the global charge transfer and the short-ranged Coulomb interactions. We suggest that a fruitful direction for future work could be to combine the ACKS2 charge distribution model with long-ranged electrostatic interactions, thus allowing the improved charge distributions obtained from ACKS2 to also result in accurate electric field screening properties.

https://doi.org/10.1021/acs.jctc.1c00975
J. Chem. Theory Comput. 2022, 18, 580−594

■ ASSOCIATED CONTENT

Supporting Information

The Supporting Information is available free of charge at https://pubs.acs.org/doi/10.1021/acs.jctc.1c00975.

ACKS2 ReaxFF parameterizations used in this study (TXT)

QEq ReaxFF parameterizations used in this study (TXT)

■ AUTHOR INFORMATION

Corresponding Author

Jason P. Koski − *Sandia National Laboratories, Albuquerque, New Mexico 87185, United States;* orcid.org/0000-0001-5740-8259; Email: jkoski@sandia.gov

Authors

Stan G. Moore − *Sandia National Laboratories, Albuquerque, New Mexico 87185, United States*

Raymond C. Clay − *Sandia National Laboratories, Albuquerque, New Mexico 87185, United States*

Kurt A. O'Hearn − *Department of Computer Science and Engineering, Michigan State University, East Lansing, Michigan 48824, United States*

H. Metin Aktulga − *Department of Computer Science and Engineering, Michigan State University, East Lansing, Michigan 48824, United States*

Mark A. Wilson − *Sandia National Laboratories, Albuquerque, New Mexico 87185, United States*

Joshua A. Rackers − *Sandia National Laboratories, Albuquerque, New Mexico 87185, United States;* orcid.org/0000-0002-8874-018X

J. Matthew D. Lane − *Sandia National Laboratories, Albuquerque, New Mexico 87185, United States;* orcid.org/0000-0002-7878-9158

Normand A. Modine − *Sandia National Laboratories, Albuquerque, New Mexico 87185, United States*

Complete contact information is available at: https://pubs.acs.org/10.1021/acs.jctc.1c00975

Notes

The authors declare no competing financial interest.

■ ACKNOWLEDGMENTS

The authors thank Louise Criscenti, Efstratios Kritikos, Andrea Giusti, and Adri van Duin for useful discussions. H.M.A. and K.A.O. acknowledge support from NSF (award number 1807622) and NIH (award number GM130641). This project was supported by LDRD project 218473. Sandia National Laboratories is a multimission laboratory managed and operated by the National Technology and Engineering Solutions of Sandia, LLC, a wholly owned subsidiary of Honeywell International, Inc., for the U.S. Department of Energy's National Nuclear Security Administration under contract DE-NA0003525. This work describes objective technical results and analysis. Any subjective views or opinions that might be expressed in the work do not necessarily represent the views of the U.S. Department of Energy or the U.S. Government.

■ REFERENCES

(1) Shaik, S.; Mandal, D.; Ramanan, R. Oriented electric fields as future smart reagents in chemistry. *Nat. Chem.* **2016**, *8*, 1091−1098.

(2) Shaik, S.; Ramanan, R.; Danovich, D.; Mandal, D. Structure and reactivity/selectivity control by oriented-external electric fields. *Chem. Soc. Rev.* **2018**, *47*, 5125−5145.

(3) Cassone, G.; Sofia, A.; Sponer, J.; Saitta, A. M.; Saija, F. Ab Initio Molecular Dynamics Study of Methanol-Water Mixtures under External Electric Fields. *Molecules* **2020**, *25*, No. 3371.

(4) Futera, Z.; English, N. J. Communication: Influence of external static and alternating electric fields on water from long-time non-equilibrium ab initio molecular dynamics. *J. Chem. Phys.* **2017**, *147*, No. 031102.

(5) Mattioli, E. J.; Bottoni, A.; Zerbetto, F.; Calvaresi, M. Oriented external electric fields affect rate and stereoselectivity of electrocyclic reactions. *J. Phys. Chem. C* **2019**, *123*, 26370−26378.

(6) Saitta, A. M.; Saija, F.; Giaquinta, P. V. Ab initio molecular dynamics study of dissociation of water under an electric field. *Phys. Rev. Lett.* **2012**, *108*, No. 207801.

(7) Han, Y.; Jiang, D.; Zhang, J.; Li, W.; Gan, Z.; Gu, J. Development, applications and challenges of ReaxFF reactive force field in molecular simulations. *Front. Chem. Sci. Eng.* **2016**, *10*, 16−38.

(8) Senftle, T. P.; Hong, S.; Islam, M. M.; Kylasa, S. B.; Zheng, Y.; Shin, Y. K.; Junkermeier, C.; Engel-Herbert, R.; Janik, M. J.; Aktulga, H. M.; Verstraelen, T.; Drama, A.; van Duin, A. C. The ReaxFF reactive force-field: development, applications and future directions. *npj Comput. Mater.* **2016**, *2*, No. 15011.

(9) Lane, J. M. D.; Leung, K.; Thompson, A. P.; Cuneo, M. E. Water desorption from rapidly-heated metal oxide surfaces-first principles, molecular dynamics, and the Temkin isotherm. *J. Phys.: Condens. Matter* **2018**, *30*, No. 465002.

(10) Koski, J. P.; Lane, J. M. D. Hydrocarbon and water desorption from iron-oxide surfaces using molecular dynamics. *AIP Conf. Proc.* **2020**, No. 070023.

(11) Rappe, A. K.; Goddard, W. A. Charge equilibration for molecular dynamics simulations. *J. Phys. Chem. A* **1991**, *95*, 3358−3363.

(12) Mortier, W. J.; Ghosh, S. K.; Shankar, S. Electronegativity-equalization method for the calculation of atomic charges in molecules. *J. Am. Chem. Soc.* **1986**, *108*, 4315−4320.

(13) Chen, J.; Martínez, T. J. QTPIE: Charge transfer with polarization current equalization. A fluctuating charge model with correct asymptotics. *Chem. Phys. Lett.* **2007**, *438*, 315−320.

(14) Verstraelen, T.; Ayers, P.; Van Speybroeck, V.; Waroquier, M. ACKS2: Atom-condensed Kohn-Sham DFT approximated to second order. *J. Chem. Phys.* **2013**, *138*, No. 074108.

(15) Assowe, O.; Politano, O.; Vignal, V.; Arnoux, P.; Diawara, B.; Verners, O.; van Duin, A. C. Reactive molecular dynamics of the initial oxidation stages of Ni (111) in pure water: effect of an applied electric field. *J. Phys. Chem. A* **2012**, *116*, 11796−11805.

(16) Chen, J.; Martínez, T. J. Charge conservation in electronegativity equalization and its implications for the electrostatic properties of fluctuating-charge models. *J. Chem. Phys.* **2009**, *131*, No. 044114.

(17) DorMohammadi, H.; Pang, Q.; Árnadóttir, L.; Isgor, O. B. Atomistic simulation of initial stages of iron corrosion in pure water using reactive molecular dynamics. *Comput. Mater. Sci.* **2018**, *145*, 126−133.

(18) Hasan, R. M. M.; Politano, O.; Luo, X. ReaxFF molecular dynamics simulation study of nanoelectrode lithography oxidation process on silicon (100) surface. *Appl. Surf. Sci.* **2019**, *496*, No. 143679.

(19) Hasan, R. M. M.; Politano, O.; Luo, X. Substrate orientation effects on nanoelectrode lithography: ReaxFF molecular dynamics and experimental study. *J. Phys. D: Appl. Phys.* **2020**, *53*, No. 295108.

(20) Fu, C. D.; He, Y.; Pfaendtner, J. Diagnosing the impact of external electric fields chemical kinetics: application to toluene oxidation and pyrolysis. *J. Phys. Chem. A* **2019**, *123*, 3080−3089.

(21) Tan, S.; Xia, T.; Shi, Y.; Pfaendtner, J.; Zhao, S.; He, Y. Enhancing the oxidation of toluene with external electric fields: a reactive molecular dynamics study. *Sci. Rep.* **2017**, *7*, No. 1710.

(22) Miao, F.; Cheng, X. Effect of electric field on polarization and decomposition of RDX molecular crystals: a ReaxFF molecular dynamics study. *J. Mol. Model.* **2020**, *26*, No. 2.

(23) Wood, M. A.; van Duin, A. C.; Strachan, A. Coupled thermal and electromagnetic induced decomposition in the molecular explosive αHMX; a reactive molecular dynamics study. *J. Phys. Chem. A* **2014**, *118*, 885−895.
(24) López-Plascencia, C. E.; Martínez-Negrete-Vera, M.; Garibay-Alonso, R. Reactive force field study of the molecular structure of water under thermal and electric effects: Water splitting phenomenon. *Int. J. Hydrogen Energy* **2017**, *42*, 4774−4781.
(25) DorMohammadi, H.; Pang, Q.; Murkute, P.; Árnadóttir, L.; Isgor, O. B. Investigation of iron passivity in highly alkaline media using reactive-force field molecular dynamics. *Corros. Sci.* **2019**, *157*, 31−40.
(26) Jiang, X. Z.; Feng, M.; Zeng, W.; Luo, K. H. Study of mechanisms for electric field effects on ethanol oxidation via reactive force field molecular dynamics. *Proc. Combust. Inst.* **2019**, *37*, 5525−5535.
(27) Gao, Q.; Han, Y.; Liang, P.; Meng, J. Influence of an external electric field on the deprotonation reactions of an Fe 3+-solvated molecule: a reactive molecular dynamics study. *Phys. Chem. Chem. Phys.* **2020**, *22*, 6291−6299.
(28) Jiang, X. Z.; Luo, K. H. Reactive and electron force field molecular dynamics simulations of electric field assisted ethanol oxidation reactions. *Proc. Combust. Inst.* **2021**, *38*, 6605−6613.
(29) Gubbels-Elzas, A.; Thijsse, B. J. Ionic motion during field-assisted oxidation of aluminium studied by molecular dynamics simulations. *Comput. Mater. Sci.* **2014**, *90*, 196−202.
(30) Jeon, B.; Van Overmeere, Q.; van Duin, A. C.; Ramanathan, S. Nanoscale oxidation and complex oxide growth on single crystal iron surfaces and external electric field effects. *Phys. Chem. Chem. Phys.* **2013**, *15*, 1821−1830.
(31) Zhang, Y.-M.; Li, J.-L.; Wang, J.-P.; Yang, X.-S.; Shao, W.; Xiao, S.-Q.; Wang, B.-Z. Research on epoxy resin decomposition under microwave heating by using ReaxFF molecular dynamics simulations. *RSC Adv.* **2014**, *4*, 17083−17090.
(32) Gergs, T.; Dirkmann, S.; Mussenbrock, T. Integration of external electric fields in molecular dynamics simulation models for resistive switching devices. *J. Appl. Phys.* **2018**, *123*, No. 245301.
(33) Gergs, T.; Schmidt, F.; Mussenbrock, T.; Trieschmann, J. Generalized Method for Charge Transfer Equilibration in Reactive Molecular Dynamics. 2020, arXiv:2006.04157. arXiv.org e-Print archive. https://arxiv.org/abs/2006.04157.
(34) Kritikos, E.; Giusti, A. Reactive Molecular Dynamics Investigation of Toluene Oxidation under Electrostatic Fields: Effect of the Modeling of Local Charge Distribution. *J. Phys. Chem. A* **2020**, *124*, 10705−10716.
(35) Chen, J.; Hundertmark, D.; Martínez, T. J. A unified theoretical framework for fluctuating-charge models in atom-space and in bond-space. *J. Chem. Phys.* **2008**, *129*, No. 214113.
(36) Chen, J. Theory and Applications of Fluctuating-Charge Models. 2010, arXiv:1004.0186. arXiv.org e-Print archive. https://arxiv.org/abs/1004.0186.
(37) O'Hearn, K. A.; Alperen, A.; Aktulga, H. M. Fast Scalable Solvers for Charge Distribution Models on Shared Memory Platforms. *SIAM J. Sci. Comput.* **2020**, *42*, C1.
(38) Grama, A.; Aktulga, H. M.; Kylasa, S. B. PuReMD, Purdue Reactive Molecular Dynamics package, 2014. https://www.cs.purdue.edu/puremd (accessed June 8, 2016).
(39) Plimpton, S. Fast Parallel Algorithms for Short-Range Molecular Dynamics. *J. Comput. Phys.* **1995**, *117*, 1−19.
(40) Thompson, A. P.; Aktulga, H. M.; Berger, R.; Bolintineanu, D. S.; Brown, W. M.; Crozier, P. S.; in'at Veld, P. J.; Kohlmeyer, A.; Moore, S. G.; Nguyen, T. D.; Shan, R.; Stevens, M. J.; Tranchida, J.; Trott, C.; Plimpton, S. J. LAMMPS-A flexible simulation tool for particle-based materials modeling at the atomic, meso, and continuum scales. *Comput. Phys. Commun.* **2021**, No. 108171.
(41) Trott, C.; Berger-Vergiat, L.; Poliakoff, D. Z.; Rajamanickam, S.; Lebrun-Grandie, D.; Madsen, J.; Gligoric, M.; Al Awar, N.; Shipman, G.; Womeldorff, G. The Kokkos EcoSystem: Comprehensive Performance Portability For High Performance Computing. *Comput. Sci. Eng.* **2021**, 10−18.
(42) Trott, C.et al. in *Kokkos 3: Programming Model Extensions for the Exascale Era*, IEEE Transactions on Parallel and Distributed Systems 2021; pp 805−817.
(43) Kokkos, 2021. https://github.com/kokkos/kokkos.
(44) Leven, I.; Hao, H.; Tan, S.; Guan, X.; Penrod, K. A.; Akbarian, D.; Evangelisti, B.; Hossain, M. J.; Islam, M. M.; Koski, J. P.; Moore, S.; Aktulga, H. M.; van Duin, A. C. T.; Head-Gordon, T. Recent Advances for Improving the Accuracy, Transferability, and Efficiency of Reactive Force Fields. *J. Chem. Theory Comput.* **2021**, *17*, 3237−3251.
(45) van Duin, A. C.; Dasgupta, S.; Lorant, F.; Goddard, W. A. ReaxFF: a reactive force field for hydrocarbons. *J. Phys. Chem. A* **2001**, *105*, 9396−9409.
(46) Aktulga, H.; Fogarty, J.; Pandit, S.; Grama, A. Parallel reactive molecular dynamics: Numerical methods and algorithmic techniques. *Parallel Comput.* **2012**, *38*, 245−259.
(47) Achtyl, J. L.; Unocic, R. R.; Xu, L.; Cai, Y.; Raju, M.; Zhang, W.; Sacci, R. L.; Vlassiouk, I. V.; Fulvio, P. F.; Ganesh, P.; Wesolowski, D. J.; Day, S.; van Duin, A. C.; Neurock, M.; Geiger, F. M. Aqueous proton transfer across single-layer graphene. *Nat. Commun.* **2015**, *6*, No. 6539.
(48) O'Hearn, K. A.; Alperen, A.; Aktulga, H. M. In *Performance Optimization of Reactive Molecular Dynamics Simulations with Dynamic Charge Distribution Models on Distributed Memory Platforms*, ICS'19: Proceedings of the Association of Computing Machinery International Conference on Supercomputing, 2019; pp 150−159.
(49) O'Hearn, K. A.; Aktulga, H. M. In *Towards Fast Scalable Solvers for Charge Equilibrationin Molecular Dynamics Applications*, 2016 7th Workshop on Latest Advances in ScalableAlgorithms for Large-Scale Systems (ScalA), 2016; pp 9−16.
(50) Chelli, R.; Procacci, P.; Righini, R.; Califano, S. Electrical response in chemical potential equalization schemes. *J. Chem. Phys.* **1999**, *111*, 8569−8575.
(51) Müser, M. H. The chemical hardness of molecules and the band gap of solids within charge equilibration formalisms. *Eur. Phys. J. B* **2012**, *85*, No. 135.
(52) Mathieu, D. Split charge equilibration method with correct dissociation limits. *J. Chem. Phys.* **2007**, *127*, No. 224103.
(53) Lee Warren, G.; Davis, J. E.; Patel, S. Origin and control of superlinear polarizability scaling in chemical potential equalization methods. *J. Chem. Phys.* **2008**, *128*, No. 144110.
(54) Nistor, R. A.; Müser, M. H. Dielectric properties of solids in the regular and split-charge equilibration formalisms. *Phys. Rev. B* **2009**, *79*, No. 104303.
(55) Verstraelen, T.; Vandenbrande, S.; Ayers, P. W. Direct computation of parameters for accurate polarizable force fields. *J. Chem. Phys.* **2014**, *141*, No. 194114.
(56) Kohn, W.; Sham, L. J. Self-Consistent Equations Including Exchange and Correlation Effects. *Phys. Rev.* **1965**, *140*, A1133−A1138.
(57) Kresse, G.; Hafner, J. Ab initio molecular dynamics for liquid metals. *Phys. Rev. B* **1993**, *47*, 558−561.
(58) Kresse, G.; Hafner, J. Ab initio molecular-dynamics simulation of the liquid-metal-amorphous-semiconductor transition in germanium. *Phys. Rev. B* **1994**, *49*, 14251−14269.
(59) Kresse, G.; Furthmüller, J. Efficiency of ab-initio total energy calculations for metals and semiconductors using a plane-wave basis set. *Comput. Mater. Sci.* **1996**, *6*, 15−50.
(60) Kresse, G.; Furthmüller, J. Efficient iterative schemes for ab initio total-energy calculations using a plane-wave basis set. *Phys. Rev. B* **1996**, *54*, 11169−11186.
(61) Perdew, J. P.; Burke, K.; Ernzerhof, M. Generalized Gradient Approximation Made Simple. *Phys. Rev. Lett.* **1996**, *77*, 3865−3868.
(62) Blöchl, P. E. Projector augmented-wave method. *Phys. Rev. B* **1994**, *50*, 17953−17979.
(63) Kresse, G.; Joubert, D. From ultrasoft pseudopotentials to the projector augmented-wave method. *Phys. Rev. B* **1999**, *59*, 1758−1775.
(64) Nosé, S. A unified formulation of the constant temperature molecular dynamics methods. *J. Chem. Phys.* **1984**, *81*, 511−519.
(65) Nosé, S. Constant Temperature Molecular Dynamics Methods. *Prog. Theor. Phys. Suppl.* **1991**, *103*, 1−46.

(66) Bylander, D. M.; Kleinman, L. Energy fluctuations induced by the Nosé thermostat. *Phys. Rev. B* **1992**, *46*, 13756−13761.
(67) Baldereschi, A. Mean-Value Point in the Brillouin Zone. *Phys. Rev. B* **1973**, *7*, 5212−5215.
(68) Smith, D. G. A.; et al. PSI4 1.4: Open-source software for high-throughput quantum chemistry. *J. Chem. Phys.* **2020**, *152*, No. 184108.
(69) Dunning, T. H. Gaussian basis sets for use in correlated molecular calculations. I. The atoms boron through neon and hydrogen. *J. Chem. Phys.* **1989**, *90*, 1007−1023.
(70) Stone, A. J. Distributed multipole analysis: Stability for large basis sets. *J. Chem. Theory Comput.* **2005**, *1*, 1128−1132.
(71) NIST Chemistry WebBook. NIST Standard Reference Database Number 69. https://webbook.nist.gov/cgi/cbook.cgi?ID=C7732185&Mask=20.
(72) Rienstra-Kiracofe, J. C.; Tschumper, G. S.; Schaefer, H. F., III; Nandi, S.; Ellison, G. B. Atomic and Molecular Electron Affinities: Photoelectron Experiments and Theoretical Computations. *Chem. Rev.* **2002**, *102*, 231−282.
(73) Chipman, D. M. Effect of molecular geometry on the electron affinity of water. *J. Phys. Chem. B* **1978**, *82*, 1080−1083.
(74) Leven, I.; Head-Gordon, T. Inertial extended-Lagrangian scheme for solving charge equilibration models. *Phys. Chem. Chem. Phys.* **2019**, *21*, 18652−18659.
(75) Leven, I.; Hao, H.; Das, A. K.; Head-Gordon, T. A Reactive Force Field with Coarse-Grained Electrons for Liquid Water. *J. Phys. Chem. Lett.* **2020**, *11*, 9240−9247.
(76) Islam, M. M.; Kolesov, G.; Verstraelen, T.; Kaxiras, E.; van Duin, A. C. EReaxFF: A Pseudoclassical Treatment of Explicit Electrons within Reactive Force Field Simulations. *J. Chem. Theory Comput.* **2016**, *12*, 3463−3472.
(77) Abrams, M. L.; Sherrill, C. D. General-order single-and multi-reference configuration interaction and coupled-cluster theory: Symmetric dissociation of water. *Chem. Phys. Lett.* **2005**, *404*, 284−288.
(78) NIST Chemistry WebBook. NIST Standard Reference Database Number 69. https://webbook.nist.gov/cgi/cbook.cgi?ID=C12385136&Mask=20.
(79) Imre, A.; Baranyi, A.; Deiters, U. K.; Kiss, P.; Kraska, T.; Quiñones Cisneros, S. E. Estimation of the Thermodynamic Limit of Overheating of Bulk Water from Interfacial Properties. *Int. J. Thermophys.* **2013**, *34*, 2053−2064.

https://doi.org/10.1021/acs.jctc.1c00975
J. Chem. Theory Comput. 2022, 18, 580−594